A measurement of the Hubble constant from Type II supernovae

T. de Jaeger[1,2]*, B. E. Stahl[1,3,4], W. Zheng[1], A. V. Filippenko[1,5], A. G. Riess[6,7], L. Galbany[8]

[1] *Department of Astronomy, University of California, Berkeley, CA 94720-3411, USA.*
[2] *Bengier Postdoctoral Fellow.*
[3] *Department of Physics, University of California, Berkeley, CA 94720-7300, USA.*
[4] *Marc J. Staley Graduate Fellow.*
[5] *Miller Senior Fellow, Miller Institute for Basic Research in Science, University of California, Berkeley, CA 94720, USA.*
[6] *Space Telescope Science Institute, 3700 San Martin Drive, Baltimore, MD 21218, USA.*
[7] *Department of Physics & Astronomy, Johns Hopkins University, Baltimore, MD 21218, USA.*
[8] *Departamento de Física Teórica y del Cosmos, Universidad de Granada, E-18071 Granada, Spain.*

ABSTRACT

Progressive increases in the precision of the Hubble-constant measurement via Cepheid-calibrated Type Ia supernovae (SNe Ia) have shown a discrepancy of $\sim 4.4\sigma$ with the current value inferred from *Planck* satellite measurements of the cosmic microwave background radiation and the standard ΛCDM cosmological model. This disagreement does not appear to be due to known systematic errors and may therefore be hinting at new fundamental physics. Although all of the current techniques have their own merits, further improvement in constraining the Hubble constant requires the development of as many independent methods as possible. In this work, we use SNe II as standardisable candles to obtain an independent measurement of the Hubble constant. Using 7 SNe II with host-galaxy distances measured from Cepheid variables or the tip of the red giant branch, we derive $H_0 = 75.8^{+5.2}_{-4.9}\,\mathrm{km\,s^{-1}\,Mpc^{-1}}$ (statistical errors only). Our value favours that obtained from the conventional distance ladder (Cepheids + SNe Ia) and exhibits a difference of $8.4\,\mathrm{km\,s^{-1}\,Mpc^{-1}}$ from the *Planck* +ΛCDM value. Adding an estimate of the systematic errors ($2.8\,\mathrm{km\,s^{-1}\,Mpc^{-1}}$) changes the $\sim 1.7\sigma$ discrepancy with *Planck* +ΛCDM to $\sim 1.4\sigma$. Including the systematic errors and performing a bootstrap simulation, we confirm that the local H_0 value exceeds the value from the early Universe with a confidence level of 95%. As in this work we only exchange SNe II for SNe Ia to measure extragalactic distances, we demonstrate that there is no evidence that SNe Ia are the source of the H_0 tension.

Key words: cosmology: distance scale – galaxies: distances and redshifts – stars: supernovae: general

1 INTRODUCTION

The current expansion rate of the Universe, known as the Hubble constant (H_0), remains one of the most important parameters in modern cosmology. Determining an accurate value is essential for obtaining information regarding our Universe, including its age and evolution. Since the discovery of the expansion of the Universe (Lemaître 1927; Hubble 1929), many efforts have been made to measure H_0 precisely and decrease its uncertainties. Traditionally, there have been two main routes for determining H_0. First, H_0 can be measured locally through the distance-ladder method. Distances to galaxies in the Hubble flow, where peculiar velocities are insignificant (the motion of galaxies is almost entirely due to the expansion of the Universe), can be measured using Type Ia supernovae (SNe Ia; e.g., Minkowski 1941; Elias et al. 1985; Filippenko 1997; Howell 2011, and references therein). For sufficiently nearby SN Ia host galaxies where individual stars can be resolved with the *Hubble Space Telescope (HST)*, the distances can be determined (and hence the peak luminosities of the SNe Ia can be calibrated) through measurements of Cepheid variable stars (Freedman et al. 2001;

* E-mail: tdejaeger@berkeley.edu

© 2020 The Authors

Sandage et al. 2006; Riess et al. 2009; Freedman & Madore 2010; Riess et al. 2011, 2016, 2018a,b; Burns et al. 2018; Dhawan et al. 2018; Riess et al. 2019) or the tip of the red giant branch (TRGB) in the Hertzsprung-Russell diagram (Madore et al. 2009; Jang & Lee 2017a,b; Freedman et al. 2019; Yuan et al. 2019). Cepheids and TRGBs can, in turn, be calibrated to geometric anchor distances like Milky Way Cepheid parallaxes (Benedict et al. 2007; Riess et al. 2014; Casertano et al. 2016), Keplerian motion of masers in NGC 4258 (Humphreys et al. 2013; Reid et al. 2019), or detached eclipsing binary stars in the Large Magellanic Cloud (Pietrzyński et al. 2013). Using this distance-ladder technique, the uncertainty in the measurement of H_0 has improved from $\sim 10\%$ (Freedman et al. 2001) to $< 2\%$ (Riess et al. 2019) during the last 20 yr. Currently, the most precise estimate of the H_0 is $74.03 \pm 1.42 \, \mathrm{km \, s^{-1} \, Mpc^{-1}}$ (Riess et al. 2019).

Second, H_0 can be predicted using the sound horizon observed from the cosmic microwave background radiation (CMB; e.g., Fixsen et al. 1996; Jaffe et al. 2001; Spergel et al. 2007; Bennett et al. 2003; Planck Collaboration et al. 2018). However, H_0 cannot be constrained directly from CMB observations. While the local H_0 value at redshift $z \approx 0$ is obtained using the distance ladder from Hubble-flow SNe Ia ($z \approx 0.02$–0.15) using calibrated objects for each step, the second value is obtained using data at $z \approx 1100$ and extrapolated to $z \approx 0$ based on the physics of the early Universe. Assuming a flat Λ cold dark matter (ΛCDM) cosmological model, Planck Collaboration et al. (2018) obtained a value of $H_0 = 67.4 \pm 0.5 \, \mathrm{km \, s^{-1} \, Mpc^{-1}}$.

Although the two H_0 values from opposite ends of the Universe agree to within 10%, their error bars do not overlap and a discrepancy of $\sim 4.4\sigma$ is seen with SNe Ia (Riess et al. 2019) (and even greater significance, exceeding 6σ, when other nearby-universe techniques are combined; Riess 2020). This disagreement does not appear to be due to known systematic errors. Independent reanalyses of the Riess et al. (2016) data have shown minimal differences (Cardona et al. 2017; Zhang et al. 2017; Feeney et al. 2018; Follin & Knox 2018; Dhawan et al. 2018; Burns et al. 2018), and as more data and independent methods are used the discrepancy is increasing (Riess et al. 2019). This significant tension between both measurements could arise from relativistic particles (dark radiation), nonzero curvature, early dark energy, increasing dark energy, or new fundamental physics.

However, to confirm the "H_0 tension" it is important to develop as many independent methods as possible having different systematic errors (see Riess 2020 for a recent review). For example, a novel measurement of H_0 has been made using quasars that are strongly gravitationally lensed into multiple images and the time-delay distance technique (Bonvin et al. 2017; Wong et al. 2019). From their analysis of multiply-imaged quasars, the H0LiCOW collaboration (Bonvin et al. 2017) has measured a value of $73.3^{+1.7}_{-1.8} \, \mathrm{km \, s^{-1} \, Mpc^{-1}}$ (Wong et al. 2019), consistent with the most recent local distance ladder measurements (Riess et al. 2019). Additionally, the Megamaser Cosmology Project, using geometric distance measurements to megamaser-hosting galaxies, obtained an independent H_0 value of $73.9 \pm 3.0 \, \mathrm{km \, s^{-1} \, Mpc^{-1}}$ (Pesce et al. 2020). Other techniques such as "standard sirens" from merger events detected through gravitational waves (Abbott et al. 2017)

are also promising, but their current precision is not sufficient to put strong constraints; there is only a single electromagnetic gravitational-wave counterpart detection ($H_0 = 70^{+12}_{-8} \, \mathrm{km \, s^{-1} \, Mpc^{-1}}$). However, even "dark sirens" that have no known electromagnetic detection have potential (Vasylyev & Filippenko 2020).

Needing approaches independent of SNe Ia, we study the use of SNe II as cosmological standardisable candles (de Jaeger et al. 2020). Observationally, SNe II are characterised by the presence of strong hydrogen features in their spectra (see Filippenko 1997, 2000 and Gal-Yam 2017 for overviews), and a plateau of varying steepness in their light curves (Barbon et al. 1979; Anderson et al. 2014; Galbany et al. 2016) during the hydrogen recombination phase. Their use as cosmic distance indicators is mainly motivated by the fact that they are more abundant than SNe Ia (Li et al. 2011; Graur et al. 2017) and their progenitors and environments are better understood than those of SNe Ia. It is now accepted that SN II progenitors arise from only one stellar population (red supergiant stars) for which the explosion mechanism is reasonably well understood (Woosley & Weaver 1995; Janka 2001; Janka et al. 2007).

At first sight, the SN II family displays a large range of peak luminosities (more than 2 mag); however, as for SNe Ia, their luminosities can be calibrated. To date, different theoretical and empirical SN II distance-measurement methods have been proposed and tested (e.g., Nugent & Hamuy 2017, and references therein). First, the expanding photosphere method based on the relation between the angular size and the ratio between its observed and theoretical flux was developed by Kirshner & Kwan (1974). Following this method, several empirical methods have developed: the standard candle method based on the correlation between the luminosity and the expansion velocities (SCM; Hamuy & Pinto 2002; de Jaeger et al. 2020), the photospheric magnitude method which corresponds to a generalisation of the SCM (PMM; Rodríguez et al. 2014, 2019), and the photometric colour method which uses the relation between the luminosity and the slope of the plateau (PCM; de Jaeger et al. 2015, 2017b). Using those techniques, H_0 values of $73 \pm 13 \, \mathrm{km \, s^{-1} \, Mpc^{-1}}$ (EPM; Schmidt et al. 1994), $69 \pm 16 \, \mathrm{km \, s^{-1} \, Mpc^{-1}}$ (SCM; Olivares E et al. 2010), and $\sim 71 \pm 8 \, \mathrm{km \, s^{-1} \, Mpc^{-1}}$ (PMM in the V band; Rodríguez et al. 2019) have been derived, but their precisions are not yet comparable to those of *Planck* or SNe Ia owing to a lack of SNe II in the Hubble flow, as well as to a small number of Cepheids or resolved red giants in SN II host galaxies.

In this work, we increase the number of calibrators and use the largest SN II sample in the Hubble flow to derive H_0 with a precision of $\sim 6.5\%$ (statistical). Section 2 contains a description of the SN data, and in Section 3 we present the methods used to derive H_0. We discuss our results in Section 4 and summarise our conclusions in Section 5.

2   DATA SAMPLE

For our analysis, we use SNe II from different surveys: the Carnegie Supernova Project-I (CSP-I[1]; Hamuy et al. 2006),

---

the Lick Observatory Supernova Search (LOSS) with the 0.76 m Katzman Automatic Imaging Telescope (KAIT[2]; Filippenko et al. 2001), the Sloan Digital Sky Survey-II SN Survey (SDSS-II[3]; Frieman et al. 2008), the Supernova Legacy Survey (SNLS[4]; Astier et al. 2006; Perrett et al. 2010), the Dark Energy Survey Supernova Program (DES-SN[5]; Bernstein et al. 2012), and the Subaru Hyper-Suprime Cam Survey (SSP-HSC; Miyazaki et al. 2012; Aihara et al. 2018). We also add SN 2009ib (Takáts et al. 2015), a nearby SN II for which we have a SN host distance measurement from Cepheids estimated by the SH0ES[6] team (A. G. Riess, 2020, private communication). All of the data have already been used in different cosmological studies (Poznanski et al. 2009, 2010; D'Andrea et al. 2010; de Jaeger et al. 2015, 2017b,a, 2020) and a complete description of the surveys is given by Poznanski et al. (2009) (KAIT-P09), D'Andrea et al. (2010) (SDSS-SN), de Jaeger et al. (2015) (CSP-I), de Jaeger et al. (2017a) (SNLS, HSC), Ganeshalingam et al. (2010); Stahl et al. (2019); de Jaeger et al. (2019) (KAIT-d19), and de Jaeger et al. (2020) (DES-SN).

Following de Jaeger et al. (2020), our method is applied at 43 d after the explosion, and only SNe II with an explosion date uncertainty smaller than 10 d are selected. Additionally, since in this work we use the SCM, at least one spectrum per SN is needed to measure the photospheric expansion velocity. After these cuts, our sample consists of 125 SNe II: 49 (CSP-I) + 13 (SDSS-SN) + 4 (SNLS) + 12 (KAIT-P09) + 30 (KAIT-d19) + 15 (DES-SN) + 1 (HSC) + 1 (SN 2009ib). Among these 125 SNe II, 89 SNe II have $z > 0.01$.

Note that all of the CMB redshifts (z_{CMB}) were obtained from the NASA/IPAC Extragalactic Database (NED[7]) and were corrected to account for peculiar flows (z_{corr}) induced by visible structures using the model of Carrick et al. (2015). A residual peculiar velocity uncertainty of $250\,km\,s^{-1}$ is also assumed.

3 METHODS

3.1 SN II standardisation

To calibrate SNe II, the SCM is applied; see de Jaeger et al. (2020) for a full description of the method. Briefly, we use the observed correlations between SN II luminosity and photospheric expansion velocity during the plateau phase as well as the colour to correct the SN II magnitude. Thus, for each SN the corrected magnitude can be written as

$$m_{corr}^X = m_X + \alpha \log_{10}\left(\frac{v_{H\beta}}{<v_{H\beta}>}\right) - \beta(c - <c>), \quad (1)$$

where X is the X-band filter, m is the apparent magnitude at 43 d, c is the colour ($<c>$ is the average colour), and $v_{H\beta}$ is the velocity measured using Hβ absorption ($<v_{H\beta}>$ is the average value). To determine the best-fitting parameters (α and β) and to derive the Hubble diagram, a Monte

Carlo Markov Chain (MCMC) simulation is performed using the Python package EMCEE developed by Foreman-Mackey et al. (2013). For more details, the reader is referred to Equations (1), (2), and (3) of de Jaeger et al. (2020).

Note that all magnitudes were simultaneously corrected for Milky Way extinction ($A_{V,G}$; Schlafly & Finkbeiner 2011), redshifts due to the expansion of the Universe (K-correction; Oke & Sandage 1968; Hamuy et al. 1993; Kim et al. 1996; Nugent et al. 2002), and differences between the photometric systems (S-correction; Stritzinger et al. 2002) using the cross-filter K-corrections defined by Kim et al. (1996). More details regarding these correction are given by Nugent et al. (2002), Hsiao et al. (2007), de Jaeger et al. (2017b), and references therein.

3.2 Calibrators

In our low-redshift samples (CSP-I, KAIT, and SN 2009ib), six SNe II have direct or indirect host-galaxy distance measurements from Cepheids, as follows.

• SN 1999em in NGC 1637 for which the distance modulus derived by Leonard et al. (2003) has been updated using the new Large Magellanic Cloud (LMC) distance (Pietrzyński et al. 2019) and an LMC to Milky Way Cepheid abundance difference of 0.30 dex (Riess et al. 2019). The distance modulus used in this work is $\mu = 30.26 \pm 0.09$ mag. Note that the metallicity term for optical Cepheid measurements used by Leonard et al. (2003) was 0.24 mag dex^{-1}.

• SN 1999gi in NGC 3184 ($\mu = 30.64 \pm 0.11$ mag; updated from Leonard et al. 2002 using the new LMC distance), which is estimated through the average of the Cepheid distances of two galaxies (NGC 3319, $\mu = 30.60 \pm 0.08$ mag; NGC 3198, $\mu = 30.68 \pm 0.08$ mag; updated from Freedman et al. 2001) associated with the same galaxy group (Tully & Fisher 1988).

• SN 2005ay in NGC 3998 ($\mu = 31.74 \pm 0.07$ mag; Riess et al. 2016), which is measured indirectly from the Cepheid distance of NGC 3982, also a member of the Ursa Major Group.

• SN 2008bk ($\mu = 27.66 \pm 0.11$ mag; Zgirski et al. 2017) in NGC 7793.

• SN 2009ib in NGC 1559 ($\mu = 31.416 \pm 0.049$ mag; A. G. Riess, 2020, private communication). This value is consistent with the one derived by Huang et al. (2020) using Mira variable stars ($\mu = 31.41 \pm 0.05$ (stat) ± 0.052 (sys) mag

• SN 2012aw in NGC 3351 ($\mu = 29.82 \pm 0.09$ mag;) updated from Kanbur et al. (2003) following the prescriptions used for SN 1999em in NGC 1637.

In addition to these six SNe II with Cepheid measurements, we also have three SNe II with TRGB distance derivations.

• SN 2004et in NGC 6946 ($\mu = 29.38 \pm 0.09$ mag; Anand et al. 2018).

• SN 2005cs in NGC 5194 (M51; $\mu = 29.62 \pm 0.09$ mag; updated from McQuinn et al. 2017).

• SN 2013ej in NGC 628 (M74; $\mu = 29.90 \pm 0.10$ mag; updated from McQuinn et al. 2017).

For SN 2005cs and SN 2013ej, to convert the TRGB luminosities to distance moduli, we used a zero-point calibration of −4.01 from outer and halo fields in NGC 4258

(Reid et al. 2019) instead of −4.06 for typical TRGB colour (Rizzi et al. 2007).

A summary of all the calibrators available in this work can be found in Table 1. To homogenise our calibrators, we remove two objects from this analysis. First, SN 2008bk, a low-luminosity SN II (Van Dyk et al. 2012), the only object for which the distance was obtained using ground-based (and not *HST*) observations (and then only of 11 Cepheids), and we cannot determine if these zero-points are consistent with those from *HST*. Second, SN 2004et has the largest Milky Way extinction ($A_{V,G} \approx 1.0$ mag), making it very unreliable. Note that Rodríguez et al. (2019) also identified SN 2004et as an outlier and they removed it from their calibrator sample.

3.3 H_0 derivation from SNe II

The method for determining H_0 can be divided into three steps. First, we need to calibrate the SN II apparent magnitudes by deriving α and β from Equation 1. To minimise the effect of peculiar-galaxy motions, we select SNe II located in the Hubble flow, with $z_{\rm corr} > 0.01$ (89 objects). Figure 1 shows the Hubble diagram for this sample. The uncertainties associated with the corrected magnitudes are

$$\sigma^2_{m_{\rm corr}} = \sigma^2_m + \left(\frac{\alpha \sigma_{v_{\rm H\beta}}}{\ln 10 v_{\rm H\beta}}\right)^2 + (\beta \sigma_{(r-i)})^2 + \sigma^2_z, \qquad (2)$$

where σ^2_z includes the redshift measurement uncertainties and a peculiar-velocity error of 250 km s^{-1}. To the total uncertainty, a free parameter $\sigma_{\rm int}$ is added to take into account the unmodelled intrinsic SN II scatter. A value of 0.27 mag is derived, consistent with previous SCM research (Poznanski et al. 2009; D'Andrea et al. 2010; de Jaeger et al. 2017a, 2020). The values of α and β used to correct the SN II apparent magnitudes are respectively $3.95^{+0.43}_{-0.42}$ and 1.07 ± 0.28 (see Section 4.1). If we assume that the colour-magnitude relation is due to extrinsic factors, the total-to-selective extinction ratio (R_V) can be obtained from β. We find a lower $R_V \approx 1$ than for SNe Ia (Folatelli et al. 2010), but the low value could be due to intrinsic magnitude-colour not properly modelled. Recently, de Jaeger et al. (2018) suggested that the majority of SN II observed colour diversity is intrinsic and not produced by host-galaxy dust extinction. Note that these parameters depend on the sample chosen; in Section 4.2, we investigate their effects on the derived value of H_0.

For the last two steps, we follow the work done by Dhawan et al. (2018) and adapt their Python programs[8] to our SN II sample. We derive the absolute magnitudes of all calibrators, $M_i^{\rm cal}$ ($\sigma_{M_i^{\rm cal}}$), using the Cepheid and TRGB distances from Table 1 and by correcting their apparent magnitudes with the α and β derived previously,

$$M_i^{\rm cal} = m_i^{\rm cal} + \alpha \log_{10}(v_{\rm H\beta}) - \beta(r-i) - \mu_{\rm cal}, \qquad (3)$$

$$\sigma_{M_i^{\rm cal}} = \sigma^2_{m_i} + \left(\frac{\alpha}{\ln 10}\frac{\sigma_{v_{\rm H\beta}}}{v_{\rm H\beta}}\right)^2 + (\beta \sigma_{(r-i)})^2 + \sigma^2_{\mu_{\rm cal}} + \sigma^2_{\rm int}. \qquad (4)$$

---

[8] https://github.com/sdhawan21/irh0/blob/master/full-analysis.ipynb
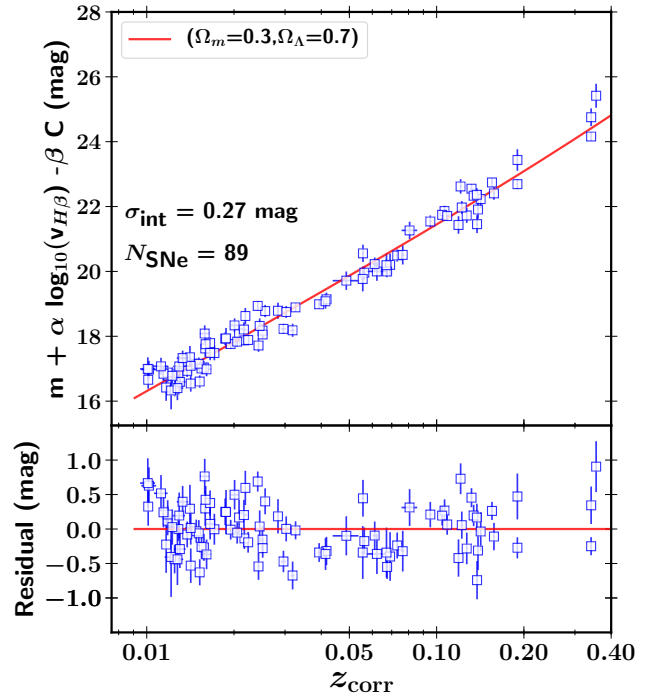
Figure 1. Hubble diagram (top) and residuals from the ΛCDM model (bottom) using the SCM as applied to our sample of 89 SNe II in the Hubble flow. $z_{\rm corr}$ corresponds to the CMB redshifts corrected to account for peculiar flows. The red solid line is the Hubble diagram for the ΛCDM model ($\Omega_m = 0.3$, $\Omega_\Lambda = 0.7$) and $H_0 = 75.8$ km s^{-1} Mpc^{-1} (see Section 4.1). This Hubble diagram was built using the i-band magnitude, ($r - i$) colour, and at 43 d after the explosion. We present the number of SNe II available at this epoch ($N_{\rm SNe}$) and the intrinsic dispersion ($\sigma_{\rm int}$). Note that the error bars do not include the intrinsic dispersion.

The absolute magnitudes for all seven calibrators are displayed in Figure 2. Note that the uncertainties include the intrinsic scatter $\sigma_{\rm int}$. The calibrators have an average weighted absolute magnitude of −16.69 mag with a dispersion of $\sigma_{\rm cal} = 0.24$ mag. The dispersion is slightly larger than that obtained using SNe Ia (0.16 mag; Riess et al. 2016; Dhawan et al. 2018) but biased by the low-statistics number of calibrators (19 calibrators used for SNe Ia). When the SCM is not applied, the dispersion increases to 0.61 mag, demonstrating the utility of the SCM. SN 2005cs exhibits the largest difference with or without SCM because SN 2005cs is a low-luminosity SN II (Pastorello et al. 2006) and has small ejecta velocities, and therefore the largest $\alpha \log_{10}$ (vel/⟨vel⟩) corrections.

It is important to note that on average, the absolute magnitude for the TRGBs is brighter ($N = 2$, -16.93 ± 0.28 mag) than for the Cepheids ($N = 5$, -16.62 ± 0.16 mag). As Jang & Lee (2017a) showed that TRGB distances are in good agreement with the Cepheid distances derived by Riess et al. (2011, 2016), the difference in absolute magnitude could be explained by a small-number statistics.

The third and last step consists of combining the calibrator and the Hubble-flow samples. The calibrator sample will constrain the absolute magnitude M_i, while the Hubble-

Table 1. Calibrator sample.

SN name	Host Galaxy	μ (mag)	calibrator	Used	references
SN 1999em	NGC 1637	30.26 ± 0.09	Cepheids	Yes	Updated from Leonard et al. (2003)
SN 1999gi	NGC 3184	30.64 ± 0.11	Cepheids	Yes	Updated from Leonard et al. (2002)
SN 2004et	NGC 6946	29.38 ± 0.09	TRGB	No	Anand et al. (2018)
SN 2005ay	NGC 3998	31.74 ± 0.07	Cepheids	Yes	Riess et al. (2016)
SN 2005cs	NGC 5194/M51	29.62 ± 0.09	TRGB	Yes	Updated from McQuinn et al. (2017)
SN 2008bk	NGC 7793	27.66 ± 0.11	Cepheids	No	Zgirski et al. (2017)
SN 2009ib	NGC 1559	31.42 ± 0.05	Cepheids	Yes	A. G. Riess (2020), priv. comm.
SN 2012aw	NGC 3351	29.82 ± 0.09	Cepheids	Yes	Updated from Kanbur et al. (2003)
SN 2013ej	NGC 628/M74	29.90 ± 0.10	TRGB	Yes	Updated from McQuinn et al. (2017)
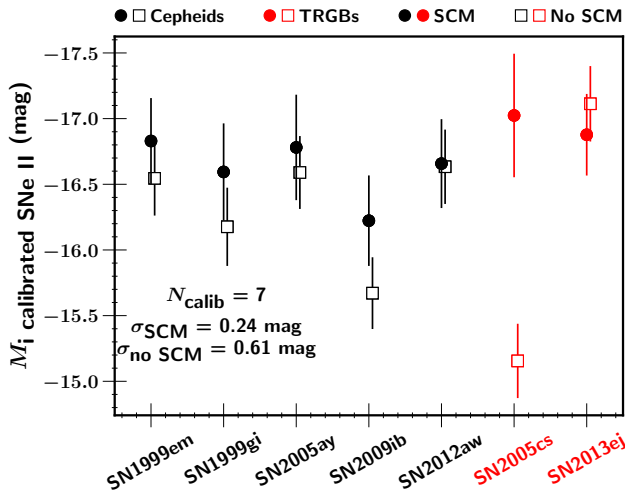
Figure 2. Absolute *i*-band magnitude 43 d after the explosion for the calibrators based on Cepheid distances (black) or the TRGB (red). The empty squares are the absolute magnitudes without applying the SCM, while the filled circles are with velocity and colour corrections. We also present the standard deviation with and without SCM.

flow sample is used to determined the intercept of the SN II magnitude-redshift relation (zero-point). In practice,

$$\mu = m_i - M_i = 5 \log_{10}(d_L) + 25, \quad (5)$$

where the luminosity distance (d_L) in Mpc is defined by its kinematic expression as

$$d_L \approx \frac{cz}{H_0}\left(1 + \frac{(1 - q_0)z}{2} + \frac{(1 - q_0 - 3q_0^2 + j_0)z^2}{6}\right). \quad (6)$$

As defined by Riess et al. (2007), q_0 is the present acceleration ($q_0 = -0.55$) and j_0 is the prior deceleration ($j_0 = 1$). Using Equations 5 and 6, we can extract H_0 as

$$\log_{10} H_0 = \frac{M_i + 5 a_i + 25}{5}, \quad (7)$$

where a_i is the intercept measured from the Hubble-flow sample and M_i is the absolute SN II *i*-band magnitude (at 43 d) derived using our calibrator sample. Following Dhawan et al. (2018), to derive H_0, we use the Python package EMCEE developed by Foreman-Mackey et al. (2013) and fit a joint model which combined the Hubble-flow and calibrator

samples. The likelihood will evaluate how close the calibrators are to the mean absolute magnitude, and simultaneously how close the Hubble-flow SN II absolute magnitudes are to the mean absolute magnitude given a value of H_0. In this model, α, β, H_0, M_i, and σ_{int} are free parameters, and a_i can be obtained using Equation 7. We run the MCMC simulation with 300 walkers and 2000 steps, and the priors are uniform for α, $\beta \neq 0$, $H_0 > 0$, and $M_i < 0$, and scale-free for $0.0 < \sigma_{\mathrm{int}}$ with $p(\sigma_{\mathrm{int}}) = 1/\sigma_{\mathrm{int}}$.

4 RESULTS

4.1 Hubble constant

In Figure 3, the one- and two-dimensional projections of the five free parameters of our model (α, β, H_0, M_i, and σ_{int}) are shown. For the Hubble-flow SN II sample, we use all SNe II with $z_{\mathrm{corr}} > 0.01$ ($N = 89$) and the seven calibrators described in Table 1. We obtain a median value of $H_0 = 75.8^{+5.2}_{-4.9}\,\mathrm{km\,s^{-1}\,Mpc^{-1}}$, where the uncertainties are only statistical. With a $\sim 6.7\%$ statistical uncertainty, this value is the most precise ever obtained using SNe II.

Our result is consistent with the local H_0 determined from SNe Ia ($74.03 \pm 1.42\,\mathrm{km\,s^{-1}\,Mpc^{-1}}$; Riess et al. 2019) and shows a discrepancy of $\sim 1.7\sigma$ with the high-redshift value ($H_0 = 67.4 \pm 0.5\,\mathrm{km\,s^{-1}\,Mpc^{-1}}$; Planck Collaboration et al. 2018). The median absolute *i*-band magnitude 43 d after the explosion of the calibrators is $M_i = -16.69 \pm 0.14\,\mathrm{mag}$ while the intercept $-5\,a_i$ has a value of $-1.08 \pm 0.04\,\mathrm{mag}$ (derived using Eq. 7). Finally, an intrinsic scatter $\sigma_{\mathrm{int}} = 0.27 \pm 0.04\,\mathrm{mag}$ is obtained, consistent with previous SCM work where the community derived a value between 0.25 and 0.33 (Poznanski et al. 2009; Olivares E et al. 2010; D'Andrea et al. 2010; de Jaeger et al. 2017a, 2020).

4.2 Systematic uncertainties

In this section, we investigate the effect of our different cuts and calibrators on H_0; the results are summarised in Table 2 and Figure 4.

First, if we change the peculiar velocity error to $150\ \mathrm{km\,s^{-1}}$ (versus $250\ \mathrm{km\,s^{-1}}$), H_0 slightly changes to $75.6^{+5.3}_{-4.9}\,\mathrm{km\,s^{-1}\,Mpc^{-1}}$, only a difference of 0.3% (0.2 $\mathrm{km\,s^{-1}\,Mpc^{-1}}$). Then, if we select only the SNe II with $z_{\mathrm{corr}} > 0.023$ (Riess et al. 2011), the number of SNe II available for the Hubble diagram decreases to 47 and H_0
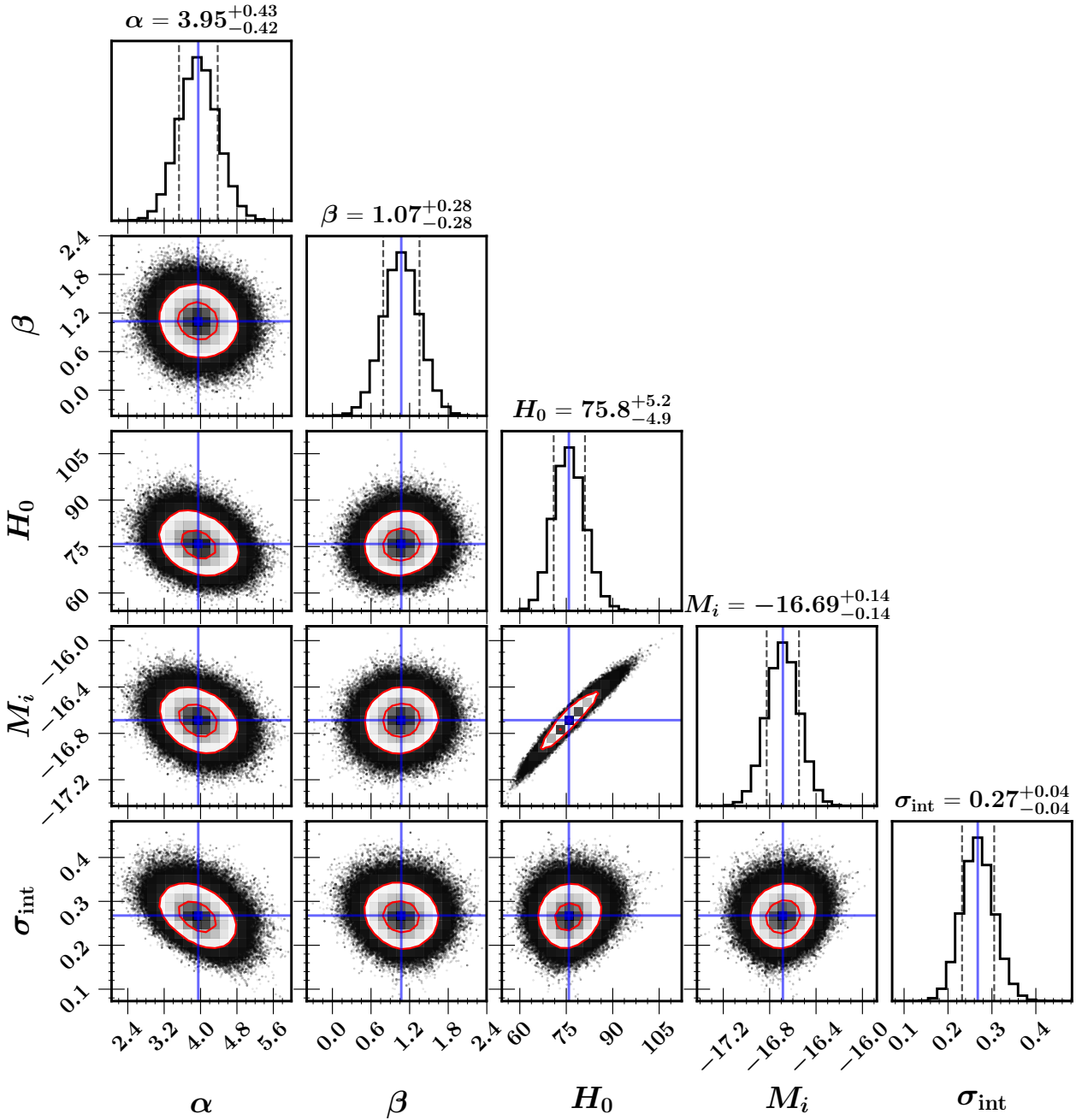
Figure 3. Corner plot showing all of the one- and two-dimensional projections. Data points are shown as grey-scale points and red contours are given at 1σ and 2σ (which corresponds in two dimensions to the 39% and 86% of the volume). The five free parameters of our model are plotted: α, β, H_0, M_i, and σ_{int}. For each parameter, the median value and the 16th and 84th percentile difference are shown. To make this figure we used the corner-plot package (triangle.py v0.1.1. Zenodo. 10.5281/zenodo.11020).

increases to $77.8^{+6.2}_{-5.7}\,\mathrm{km\,s^{-1}\,Mpc^{-1}}$, a difference of 2.6% ($1.9\,\mathrm{km\,s^{-1}\,Mpc^{-1}}$).

The largest difference in H_0 is seen when different calibrators are used. If only the Cepheids are selected as calibrators, H_0 increases to $78.5^{+6.3}_{-5.8}\,\mathrm{km\,s^{-1}\,Mpc^{-1}}$, a difference of 3.2% compared with the original sample. With the Cepheids, a slight difference of 0.5% from the original sample is also seen for the absolute i-band magnitude: -16.61 ± 0.16 mag. As discussed in Section 3.3 and Figure 2, SN II magnitudes calibrated with TRGBs are on average brighter than those

calibrated using Cepheids. Therefore, if only the TRGBs are used as calibrators, the absolute i-band magnitude increases to -16.89 ± 0.27 mag, a difference of 0.20 mag from the original sample. Although the dispersion decreases to 0.08 mag (instead of 0.24 mag), H_0 decreases to $69.0^{+9.1}_{-8.2}\,\mathrm{km\,s^{-1}\,Mpc^{-1}}$, a difference of 9.0%. However, the large difference is driven by small-number statistics.

By removing the least luminous SN II (SN 2009ib; see Fig. 2) from the Cepheid sample, we derive a value smaller than that obtained with the original sample,

$74.9^{+6.7}_{-6.1}$ km s^{-1} Mpc^{-1}, a difference of only 0.9 km s^{-1} Mpc^{-1} ($\sim 1.2\%$). However, the absolute-magnitude dispersion of the calibrators decreases to 0.10 mag (versus 0.21 mag) but with only 4 SNe II. We can also combine the Cepheid and TRGB samples after removing SN 2009ib. The calibrator absolute magnitude dispersion remains small (0.14 mag) and the H$_0$ derived presents a difference of only 2.9 km s^{-1} Mpc^{-1} (3.8%). As a test, we also add the two calibrators (SN 2004et and SN 2008bk) removed from our calibrator set (see Section 3.2). With the nine calibrators we obtain a value of $74.4^{+4.8}_{-4.5}$ km s^{-1} Mpc^{-1}, which differs by 1.4 km s^{-1} Mpc^{-1} ($\sim 1.8\%$)

To get a more realistic idea of the calibrator effects on H$_0$, we also perform a bootstrap resampling of the set of calibrators, with replacement (see Figure 5). To explore all the possibilities (13!/7!6!), we run 1716 simulations and get an average value of 76.1 ± 4.2 km s^{-1} Mpc^{-1}. To compare with the original value, we take the median of these simulations, and as total uncertainty the standard deviation (4.2 km s^{-1} Mpc^{-1}) added in quadrature to the mean of the errors obtained for each simulation (+5.3 and −5.00 km s^{-1} Mpc^{-1}). We derive H$_0$ close to the original value: $75.4^{+6.8}_{-6.5}$ km s^{-1} Mpc^{-1}, differing by only 0.4 km s^{-1} Mpc^{-1} ($\sim 0.5\%$). The distribution displayed in Figure 5 clearly shows that our H$_0$ value favours that obtained by Riess et al. (2019). The peak of our distribution matches H$_0$ from the local measurements using SNe Ia while the distribution almost does not overlap the *Planck*+ΛCDM value. The fact that our distribution extends to large H$_0$ values (85–95 km s^{-1} Mpc^{-1}) is driven by SN 2009ib, which is the faintest calibrator. All the values larger than 85 km s^{-1} Mpc^{-1} were obtained when among the seven selected calibrators, SN 2009ib is used at least four times. For example, among the 1716 different possibilities, as we select seven SNe (with replacement) from our set of calibrators, for some combinations we used [SN 2009ib, SN 2009ib, SN 2009ib, SN 2009ib, X, Y, Z], where X, Y, and Z are SN 1999em, SN 1999gi, SN 2005ay, SN 2005cs, SN 2009ib, SN 2012aw, or SN 2013ej.

Finally, we can select different surveys to calibrate the SNe II. If we select only CSP-I (37 SNe II), H$_0$ is very consistent with the original sample value with a slight difference of 0.4 km s^{-1} Mpc^{-1} ($\sim 0.5\%$). Combining our two low-redshift samples (CSP-I and KAIT) or selecting only KAIT decreases the value to (respectively) $74.7^{+6.1}_{-5.6}$ km s^{-1} Mpc^{-1} and $75.6^{+5.4}_{-5.0}$ km s^{-1} Mpc^{-1}; these are respective differences of 1.1 km s^{-1} Mpc^{-1} and 0.2 km s^{-1} Mpc^{-1} (1.5% and 0.3%). If we select only the "high-z" sample (SDSS-SN, SNLS, DES-SN, HSC), H$_0$ increases to $78.1^{+6.0}_{-5.6}$ km s^{-1} Mpc^{-1}, a difference of 2.3 km s^{-1} Mpc^{-1} (3.0%).

From the standard deviation of 13 analysis variants presented in Table 2, we derive a systematic uncertainty of ~ 2.5 km s^{-1} Mpc^{-1} (i.e., 3.3%). To this systematic uncertainty, we also add in quadrature an uncertainty of ~ 1.2 km s^{-1} Mpc^{-1} (1.5% for the LMC in Table 6 of Riess et al. 2019) owing to the error in the anchor measurements (anchor distance, mean of period-luminosity relation in anchor, zero-points anchor-to-hosts, and Cepheid metallicity). The total systematic uncertainty is ~ 2.8 km s^{-1} Mpc^{-1} (i.e., 3.7%). Thus, from our original sample, we obtain H$_0$ = $75.8^{+5.2 \text{ (stat)}}_{-4.9 \text{ (stat)}} \pm 2.8$ (sys) km s^{-1} Mpc^{-1}. Our H$_0$ value

(75.8 ± 5.8 km s^{-1} Mpc^{-1}) derived using SNe II is consistent (difference of 0.3σ) with the local measurements from SNe Ia (Riess et al. 2019) but show a discrepancy of $\sim 1.4\sigma$ with the high-redshift results (Planck Collaboration et al. 2018). Therefore, our value favours that obtained by Riess et al. (2019) (with a difference of only 1.8 km s^{-1} Mpc^{-1}) rather than that estimated by Planck Collaboration et al. (2018) (with a difference of 8.4 km s^{-1} Mpc^{-1}). Note that the small calibrator set leads to large statistical uncertainty but leaves room for decreasing the total uncertainty. As a simple test, instead of selecting seven calibrators, we use each calibrator twice (14 calibrators in total). The final statistical uncertainty decreases from 5.1 (the average of 5.2 and 4.9) to 3.7 km s^{-1} Mpc^{-1} (25%).

To summarise, in this work we only exchange SNe II for SN Ia to measure extragalactic distances; taking this study at face-value, there is no evidence that SNe Ia are the source of the H$_0$ tension. The probability $P(H_0 \leq H_{0,Planck})$ that our H$_0$ measurement from the bootstrap distribution (moved toward the *Planck* measurement by the systematic error) is at least as low as 67.4 km s^{-1} Mpc^{-1} (Planck Collaboration et al. 2018) is only 4.5% (see Eq. 10 of Pesce et al. 2020).

5 CONCLUSIONS

In this work, we show that SNe II have a role to play in the "H$_0$ tension," as they can be used to obtain extragalactic distances and provide an independent measurement of H$_0$. From SNe II and using only seven objects with Cepheid or TRGB independent host-galaxy distance measurements, we derive the most precise value of H$_0$ solely using SNe II: H$_0$ = $75.8^{+5.2}_{-4.9}$ km s^{-1} Mpc^{-1}, where the uncertainties are only statistical.

We also investigate the effect of our different cuts and calibrators on H$_0$ and estimate a systematic error of ~ 2.8 km s^{-1} Mpc^{-1} ($\sim 3.7\%$). If we combine the systematic and the statistical errors, our value (75.8 ± 5.8 km s^{-1} Mpc^{-1}) is consistent with the local measurement (Riess et al. 2019), a difference of only 1.8 km s^{-1} Mpc^{-1}. However, our H$_0$ value differs by 1.4σ from the high-redshift results (Planck Collaboration et al. 2018) – a difference of 8.4 km s^{-1} Mpc^{-1}. The probability that our H$_0$ measurement from the bootstrap distribution is at least as low as 67.4 km s^{-1} Mpc^{-1} (Planck Collaboration et al. 2018) is only 4.5%. Given that we only exchange SNe II for SNe Ia, this demonstrates that there is no evidence from our work that SNe Ia are the source of the H$_0$ tension.

With the next generation of telescopes (e.g., the Vera C. Rubin Observatory), we will be able to increase the number of calibrators and SNe II in the Hubble flow and thus improve the precision of H$_0$.

Table 2. Free-parameter values for different sample choices.

Sample	Cali	$N_{\rm cali}$	$\sigma_{\rm cali}$ (mag)	$N_{\rm SNe}$	α	β	H_0 (km s^{-1} Mpc^{-1})	M_i (mag)	$-5\,a_i$ (mag)	$\sigma_{\rm int}$ (mag)	ΔH_0
Original	C+T	7	0.24	89	$3.95^{+0.43}_{-0.42}$	1.07 ± 0.28	$75.8^{+5.2}_{-4.9}$	-16.69 ± 0.14	-1.08 ± 0.04	0.27 ± 0.04	$\cdots$
$v_{\rm pec}=150$ km s^{-1}	C+T	7	0.24	89	$3.94^{+0.43}_{-0.42}$	$1.07^{+0.28}_{-0.27}$	$75.6^{+5.3}_{-4.9}$	-16.69 ± 0.14	-1.08 ± 0.04	0.28 ± 0.04	0.3%
$z_{\rm corr} > 0.023$	C+T	7	0.29	47	$4.07^{+0.65}_{-0.63}$	$0.41^{+0.48}_{-0.46}$	$77.8^{+6.2}_{-5.7}$	-16.79 ± 0.16	-1.24 ± 0.05	$0.28^{+0.05}_{-0.04}$	2.6%
$0.023 > z_{\rm corr} > 0.15$	C+T	7	0.27	40	$4.08^{+0.74}_{-0.72}$	$0.71^{+0.50}_{-0.49}$	$78.2^{+6.3}_{-5.8}$	-16.74 ± 0.16	-1.20 ± 0.06	0.29 ± 0.05	3.2%
$z_{\rm corr} > 0.01$	C	5	0.21	89	$4.02^{+0.46}_{-0.45}$	$1.05^{+0.28}_{-0.29}$	$78.5^{+6.3}_{-5.8}$	-16.61 ± 0.16	-1.08 ± 0.04	0.27 ± 0.04	3.6%
$z_{\rm corr} > 0.01$	T	2	0.08	89	$3.96^{+0.44}_{-0.42}$	$1.00^{+0.30}_{-0.29}$	$69.0^{+9.1}_{-8.2}$	-16.89 ± 0.27	-1.09 ± 0.04	0.27 ± 0.04	9.0%
$-$09ib	C	4	0.10	89	$4.00^{+0.45}_{-0.44}$	$1.01^{+0.28}_{-0.29}$	$74.9^{+6.7}_{-6.1}$	-16.71 ± 0.18	-1.08 ± 0.04	0.27 ± 0.04	1.2%
$-$09ib	C+T	6	0.14	89	$3.94^{+0.42}_{-0.41}$	$1.03^{+0.28}_{-0.29}$	$72.9^{+5.4}_{-5.0}$	-16.77 ± 0.15	-1.08 ± 0.04	0.27 ± 0.04	3.8%
+04et, 08bk	C+T	9	0.35	89	$4.16^{+0.43}_{-0.42}$	$1.15^{+0.28}_{-0.29}$	$74.4^{+4.8}_{-4.5}$	-16.73 ± 0.13	-1.08 ± 0.04	0.27 ± 0.03	1.8%
bootstrap	C+T	7	0.18	89	$3.96^{+0.45}_{-0.44}$	$1.04^{+0.28}_{-0.27}$	$75.4^{+6.8}_{-6.5}$	-16.70 ± 0.18	-1.08 ± 0.04	0.27 ± 0.04	0.5%
CSP-I	C+T	7	0.23	37	$3.86^{+0.58}_{-0.56}$	$1.18^{+0.41}_{-0.40}$	$76.2^{+5.4}_{-4.9}$	-16.62 ± 0.14	-1.03 ± 0.05	0.24 ± 0.04	0.5%
KAIT	C+T	7	0.27	19	$4.75^{+0.56}_{-0.93}$	$1.95^{+0.53}_{-0.56}$	$74.7^{+6.1}_{-5.6}$	-16.59 ± 0.14	-0.96 ± 0.08	0.26 ± 0.07	1.5%
CSP-I+KAIT	C+T	7	0.23	56	$4.10^{+0.54}_{-0.50}$	$1.39^{+0.34}_{-0.35}$	$75.6^{+5.4}_{-5.0}$	-16.62 ± 0.14	-1.01 ± 0.05	0.26 ± 0.05	0.3%
"high-z"	C+T	7	0.26	33	$3.61^{+0.67}_{-0.64}$	$0.56^{+0.50}_{-0.49}$	$78.1^{+6.0}_{-5.6}$	-16.74 ± 0.15	-1.21 ± 0.06	0.27 ± 0.05	3.0%

Effect of systematic errors on the best-fitting values using the SCM and different samples. Original line corresponds to the values obtained in Section 4.1. We try different cuts in redshift ($z_{\rm corr}$), surveys (e.g., only CSP-I, only KAIT, CSP-I+KAIT, high-z SDSS+SNLS+DES+HSC), calibrators [Cepheids (C) and/or TRGBs (T)], and also remove or add some calibrators (e.g., $-$09ib for SN 2009ib; +04et, 08bk for SN 2004et, SN 2008bk). The last line corresponds to the average value obtained when performed a bootstrap resampling of the set of calibrators, with replacement using seven calibrators. For each parameter, the median value with the 16th and 84th percentile differences are given. For the last line, the median and the standard deviation added in quadrature to the mean of the uncertainties obtained for each parameter are written. Note that the uncertainties are only statistical. The last column, ΔH_0, corresponds to the percentage difference from the original.
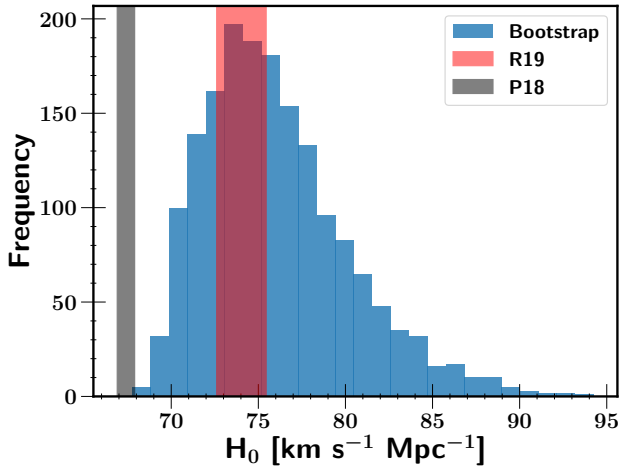
Figure 4. Comparison of the H₀ value derived in this work using SNe II with different cuts or samples (bottom black squares). The red filled region corresponds to the value obtained from our "original" sample ($z_{corr} > 0.01$, $v_{pec} = 250\,\mathrm{km\,s^{-1}}$, and using our seven calibrators). We also added the local measurements from SNe Ia (blue circles) using optical colours (Riess et al. 2011, 2016, 2019), the Riess et al. 2016 data reanalysis (Cardona et al. 2017; Zhang et al. 2017; Feeney et al. 2018), using near-infrared (NIR) filters (Dhawan et al. 2018; Burns et al. 2018), with TRGB + SNe Ia (Freedman et al. 2019), TRGB + SNe Ia with OGLE LMC reddening (Yuan et al. 2019), and with Mira variables + SNe Ia (Huang et al. 2020). Published values using SNe II from Schmidt et al. (1994), Olivares E et al. (2010), and Rodríguez et al. (2019) are also shown (top black squares). H₀ values estimated using 6 masers in the Hubble flow (Pesce et al. 2020), infrared Tully-Fisher relation (Kourkchi et al. 2020), the independent methods of quasar strong lensing (Wong et al. 2019), and gravitational-wave sources (Abbott et al. 2017) are also presented (dark cyan down-pointing triangle, magenta diamond, brown up-pointing triangle, and green left-pointing triangle, respectively). Finally, the high-z value predicted by the CMB data + ΛCDM from Planck Collaboration et al. (2018) is represented by an orange right-pointing triangle.

Figure 5. Histogram of our bootstrap resampling of the set of calibrators, with replacement. In total, 1716 simulations were performed and 25 bins are used. An average value of $76.1 \pm 4.2\,\mathrm{km\,s^{-1}\,Mpc^{-1}}$ and a median value of $75.4\,\mathrm{km\,s^{-1}\,Mpc^{-1}}$ are derived. The red and black filled regions correspond to the H_0 values obtained (respectively) by Riess et al. (2019) and Planck Collaboration et al. (2018). None of the 1716 H_0 values are smaller than 67.4 $\mathrm{km\,s^{-1}\,Mpc^{-1}}$ (Planck Collaboration et al. 2018) and only 3.5% have a discrepancy smaller than 1σ (including only a systematic error of $2.8\,\mathrm{km\,s^{-1}\,Mpc^{-1}}$).

REFERENCES

Abbott B. P., Abbott R., Abbott T. D., et al. 2017, Nature, 551, 85

Aihara H., Armstrong, R., Bickerton, S., et al. 2018, PASJ, 70, S4

Anand G. S., Rizzi L., Tully R. B., 2018, AJ, 156, 105

Anderson J. P., González-Gaitán S., Hamuy M., et al. 2014, ApJ, 786, 67

Astier P., Guy J., Regnault N., et al. 2006, A&A, 447, 31

Barbon R., Ciatti F., Rosino L., 1979, A&A, 72, 287

Benedict G. F., McArthur B. E., Feast M. W., et al. 2007, AJ, 133, 1810

Bennett C. L., Hill R. S., Hinshaw G., et al. 2003, ApJS, 148, 1

Bernstein J. P., Kessler R., Kuhlmann S., et al. 2012, ApJ, 753, 152

Bonvin V., Courbin, F., Suyu, S. H., et al. 2017, MNRAS, 465, 4914

Burns C. R., Parent, E., Phillips, M. M., et al. 2018, ApJ, 869, 56

Cardona W., Kunz M., Pettorino V., 2017, J. Cosmology Astropart. Phys., 3, 056

Carrick J., Turnbull S. J., Lavaux G., Hudson M. J., 2015, MNRAS, 450, 317

Casertano S., Riess, A. G., Anderson, J., et al. 2016, ApJ, 825, 11

D'Andrea C. B., Sako M., Dilday B., et al. 2010, ApJ, 708, 661

de Jaeger T., Galbany L., Filippenko A. V., et al. 2017a, MNRAS, 472, 4233

de Jaeger T., González-Gaitán S., Anderson J. P., et al. 2015, ApJ, 815, 121

de Jaeger T., González-Gaitán S., Hamuy M., et al. 2017b, ApJ, 835, 166

de Jaeger T., Anderson, J. P., Galbany, L., et al. 2018, MNRAS, 478, 3776

de Jaeger T., Zheng, W., Stahl, B. E., et al. 2019, MNRAS, 490, 2799

de Jaeger T., Galbany, L., González-Gaitán, S., et al. 2020, MNRAS,

Dhawan S., Jha S. W., Leibundgut B., 2018, A&A, 609, A72

Elias J. H., Matthews K., Neugebauer G., Persson S. E., 1985, ApJ, 296, 379

Feeney S. M., Mortlock D. J., Dalmasso N., 2018, Monthly Notices of the Royal Astronomical Society, 476, 3861

Filippenko A. V., 1997, ARA&A, 35, 309

Filippenko A. V., 2000, in Holt S. S., Zhang W. W., ed., American Institute of Physics Conference Series Vol. 522, 123 (arXiv:astro-ph/0002264), doi:10.1063/1.1291705

Filippenko A. V., Li W. D., Treffers R. R., Modjaz M., 2001, in Paczynski B., Chen W.-P., Lemme C., ed., Astronomical Society of the Pacific Conference Series Vol. 246, 121

Fixsen D. J., Cheng E. S., Gales J. M., et al. 1996, ApJ, 473, 576

Folatelli G., Phillips M. M., Burns C. R., et al. 2010, AJ, 139, 120

Follin B., Knox L., 2018, MNRAS, 477, 4534

Foreman-Mackey D., Hogg D. W., Lang D., Goodman J., 2013, PASP, 125, 306

Freedman W. L., Madore B. F., 2010, ARA&A, 48, 673

Freedman W. L., Madore B. F., Gibson B. K., et al. 2001, ApJ, 553, 47

Freedman W. L., Madore, B. F., Hatt, D., et al. 2019, ApJ, 882, 34

Frieman J. A., Bassett B., Becker A., et al. 2008, AJ, 135, 338

Galbany L., Hamuy M., Phillips M. M., et al. 2016, AJ, 151, 33

Gal-Yam A., 2017, in Handbook of Supernovae, ed. Alsabti, A. W. & Murdin, P., 195, doi:10.1007/978-3-319-21846-5_35

Ganeshalingam M., Li W., Filippenko A. V., et al. 2010, ApJS, 190, 418

Graur O., Bianco F. B., Modjaz M., Shivvers I., Filippenko A. V., Li W., Smith N., 2017, ApJ, 837, 121

Hamuy M., Folatelli G., Morrell N. I., et al. 2006, PASP, 118, 2

Hamuy M., Phillips M. M., Wells L. A., Maza J., 1993, PASP, 105, 787

Hamuy M., Pinto P. A., 2002, ApJ, 566, L63

Howell D. A., 2011, Nature Communications, 2, 350

Hsiao E. Y., Conley A., Howell D. A., et al. 2007, ApJ, 663, 1187

Huang C. D., Riess, A. G., Yuan, W., et al. 2020, ApJ, 889, 5

Hubble E., 1929, Proceedings of the National Academy of Science, 15, 168

Humphreys E. M. L., Reid M. J., Moran J. M., Greenhill L. J., Argon A. L., 2013, ApJ, 775, 13

Jaffe A. H., Ade P. A., Balbi A., et al. 2001, Physical Review Letters, 86, 3475

Jang I. S., Lee M. G., 2017a, ApJ, 835, 28

Jang I. S., Lee M. G., 2017b, ApJ, 836, 74

Janka H.-T., 2001, A&A, 368, 527

Janka H.-T., Langanke K., Marek A., Martínez-Pinedo G., Müller B., 2007, Phys. Rep., 442, 38

Kanbur S. M., Ngeow C., Nikolaev S., Tanvir N. R., Hendry M. A., 2003, A&A, 411, 361

Kim A., Goobar A., Perlmutter S., 1996, PASP, 108, 190

Kirshner R. P., Kwan J., 1974, ApJ, 193, 27

Kourkchi E., Tully R. B., Anand G. S., Courtois H. M., Dupuy A., Neill J. D., Rizzi L., Seibert M., 2020, arXiv e-prints, p. arXiv:2004.14499

Lemaître G., 1927, Annales de la Société Scientifique de Bruxelles, 47, 49

Leonard D. C., Filippenko A. V., Li W., et al. 2002, AJ, 124, 2490

Leonard D. C., Kanbur S. M., Ngeow C. C., Tanvir N. R., 2003, ApJ, 594, 247

Li W., Leaman J., Chornock R., et al. 2011, MNRAS, 412, 1441

Madore B. F., Mager V., Freedman W. L., 2009, ApJ, 690, 389

McQuinn K. B. W., Skillman E. D., Dolphin A. E., Berg D., Kennicutt R., 2017, AJ, 154, 51

Minkowski R., 1941, PASP, 53, 224

Miyazaki S., Komiyama, Y., Nakaya, H., et al. 2012, Proc. SPIE, 8446, 84460Z

Nugent P., Hamuy M., 2017, in Handbook of Supernovae, ed. Alsabti, A. W. & Murdin, P., 2671, doi:10.1007/978-3-319-21846-5_108

Nugent P., Kim A., Perlmutter S., 2002, PASP, 114, 803

Oke J. B., Sandage A., 1968, ApJ, 154, 21

Olivares E F., Hamuy M., Pignata G., et al. 2010, ApJ, 715, 833

Pastorello A., Sauer D., Taubenberger S., Mazzali P. A., et al. 2006, MNRAS, 370, 1752

Perrett K., Balam D., Sullivan M., et al. 2010, AJ, 140, 518

Pesce D. W., Braatz, J. A., Reid, M. J., et al. 2020, ApJ, 891, L1

Pietrzyński G., Graczyk, D., Gieren, W., et al. 2013, Nature, 495, 76

Pietrzyński G., Graczyk, D., Gallenne, A., et al. 2019, Nature, 567, 200

Planck Collaboration, Aghanim, N., Akrami, Y., et al. 2018, arXiv e-prints, parXiv:1807.06209

Poznanski D., Butler N., Filippenko A. V., et al. 2009, ApJ, 694, 1067

Poznanski D., Nugent P. E., Filippenko A. V., 2010, ApJ, 721, 956

Reid M. J., Pesce D. W., Riess A. G., 2019, ApJ, 886, L27

Riess A. G., 2020, Nature Reviews Physics, 2, 10

Riess A. G., Strolger, L.-G., Casertano, S., et al. 2007, ApJ, 659, 98

Riess A. G., Macri, L., Casertano, S., et al. 2009, ApJ, 699, 539

Riess A. G., Casertano S., Anderson J., MacKenty J., Filippenko A. V., 2014, ApJ, 785, 161

Riess A. G., Casertano S., Yuan W., et al. 2018a, ApJ, 855, 136

Riess A. G., Casertano S., Yuan W., Macri L. M., Scolnic D., 2019, ApJ, 876, 85

Riess A. G., Macri L., Casertano S., et al. 2011, ApJ, 730, 119

Riess A. G., Macri L., Hoffmann S. L., et al. 2016, ApJ, 826, 56

Riess A. G., Casertano, S., Yuan, W., et al. 2018b, ApJ, 861, 126

Rizzi L., Tully R. B., Makarov D., Makarova L., Dolphin A. E., Sakai S., Shaya E. J., 2007, ApJ, 661, 815

Rodríguez Ó., Clocchiatti A., Hamuy M., 2014, AJ, 148, 107

Rodríguez Ó., Pignata, G., Hamuy, M., et al. 2019, MNRAS, 483, 5459

Sandage A., Tammann G. A., Saha A., Reindl B., Macchetto F. D., Panagia N., 2006, ApJ, 653, 843

Schlafly E. F., Finkbeiner D. P., 2011, ApJ, 737, 103

Schmidt B. P., Kirshner R. P., Eastman R. G., et al. 1994, ApJ, 432, 42

Spergel D. N., Bean R., Doré O., et al. 2007, ApJS, 170, 377

Stahl B. E., Zheng W., de Jaeger T., et al. 2019, MNRAS, 490, 3882

Stritzinger M., Hamuy M., Suntzeff N. B., et al. 2002, AJ, 124, 2100

Takáts K., Pumo, M. L., Elias-Rosa, N., et al. 2015, MNRAS, 450, 3137

Tully R. B., Fisher J. R., 1988, Catalog of Nearby Galaxies

Van Dyk S. D., Davidge, T. J., Elias-Rosa, N., et al. 2012, AJ, 143, 19

Vasylyev S. S., Filippenko A. V., 2020, ApJ, submitted

Wong K. C., et al. 2019, arXiv e-prints, p. arXiv:1907.04869

Woosley S. E., Weaver T. A., 1995, ApJS, 101, 181

Yuan W., Riess A. G., Macri L. M., Casertano S., Scolnic D. M., 2019, ApJ, 886, 61

Zgirski B., Gieren, W., Pietrzyński, G., et al. 2017, ApJ, 847, 88

Zhang B. R., Childress M. J., Davis T. M., Karpenka N. V., Lidman C., Schmidt B. P., Smith M., 2017, MNRAS, 471, 2254

This paper has been typeset from a TEX/LATEX file prepared by the author.